Egypt. J. Bot. **Vol. 62**, No. 2, pp. - (2022)

Egyptian Journal of Botany
http://ejbo.journals.ekb.eg/

Biosynthesis, Characterization, and Assessment of Zirconia Nanoparticles by *Fusarium oxysporum* species as Potential Novel Antimicrobial and Cytotoxic Agents

Ashraf Elsayed[(1)#], Ghada M. El-Shamy[(2)#], Attia A. Attia[(2)]
[(1)]Department of Botany, Faculty of Science, Mansoura University, Mansoura, PO. 35516, Egypt; [(2)]Department of Botany and Microbiology, Faculty of Science, Benha University, Benha, Egypt.

ZIRCONIA nanoparticles (ZrNPs) were efficiently biosynthesized by *Fusarium oxysporum*. The formation of ZrNPs was characterized by UV-visible spectral analysis, transmission electron microscopy, selected area diffraction pattern analysis, scanning electron microscopy, energy-dispersive X-ray analysis, and FT-IR spectroscopy. The results identified the generation of ZrNPs by the transformation of zirconia cations in the solution into zirconium dioxide in the nanosized particles with narrow size distribution. ZrNPs had moderate cytotoxic effects on HePG-2 (IC_{50}= 32.38µg/mL), MCF-7 (IC_{50}= 47.19µg/mL), PC3 (IC_{50}= 43.50µg/mL), HeP2 (IC_{50}= 38.23µg/mL), and HeLa (IC_{50}= 33.62µg/mL) cell lines, complemented by weak cytotoxicity in HCT-116 (IC_{50}= 58.13µg/mL) and normal WI-38 cell lines (IC_{50}= 58.51µg/mL). Finally, the antimicrobial activity of ZrNPs was evaluated, in which the results indicated a minimum inhibitory concentration value at 50 µg/mL in the tests against *K. pneumoniae*, *E. coli*, and *C. albicans*, whereas the MIC value was recorded at 25µg/mL against *S. aureus*.

Keywords: Antimicrobial potency, Biogenic nanozirconia, Cytotoxicity, *Fusarium oxysporum*, Spectroscopic analysis.

Introduction

Developing consistent techniques for the synthesis of nanoparticles is of important significance (Osborne et al., 2012; Valencia et al., 2012; Singh et al., 2016) and has increased interest by researchers with biological and medical systems, including frequently synthesized biomaterials (Hamouda, 2012; Hayat et al., 2019). Recently, there has been increasing attention to the synthesis of metal nanoparticles using various methods (Panigrahi et al., 2004; Iravani et al., 2014; Jamkhande et al., 2019), but eco-friendly approaches remain the most important because of the ease of preparing nanoparticles with high efficiency (Bhardwaj et al., 2020; Gaafar et al., 2020) as well as the use of extracts prepared from microorganisms (Ingale & Chaudhari, 2013; Patil & Kim, 2018). As an essential branch of nanotechnology, nanoparticles are of considerable biological importance because they increase the efficiency of plant extracts and those prepared using microorganisms. Metal nanoparticles are also beneficial as they have magnetic, electronic, and optical properties that differ depending on the size, charge, distribution, and composition nature. Conversely, the biosynthesis of these nanoparticles using microorganisms in many techniques has received great attention because of their efficacy in many applications (Sarma et al., 2021).

The biogenic origin of zirconia nanoparticles (ZrNPs) has recently fascinated researchers; these nanoparticles can be biosynthesized and applied in different manners, including as the adsorption of methylene blue dye (Alagarsamy et

[#]Corresponding author Ashraf Elsayed email: ashraf-badawy@mans.edu.eg; Tel. +201069060801; ORCID ID: https://orcid.org/0000-0003-2122-767X. [#]Corresponding author Ghada M. El-Shamy e-mail: ghadaelshamy18@gmail.com
Received 01/01/ 2022; Accepted 29/03/ 2022
DOI: 10.21608/ejbo.2022.114070.1869
Edited by: Prof. Dr. Ghanem, Khaled M., Faculty of Science, Alexandria University, Alexandira, Egypt.

al., 2022), rubber latex fuel by nickel anesthetized zirconium dioxide nanoparticles (Yadav et al., 2021), adsorptive properties of ZrNPs prepared from *Euclea natalensis* plant extract (da Silva et al., 2019), antimicrobial properties of ZrNPs prepared from *Laurus nobilis* extract (Chau et al., 2021), oxidative stress-mediated cytotoxicity (Asadpour et al., 2016), and the biological profiles of zirconium dioxide nanoparticles (Almjasheva et al., 2017).

ZrNPs are chemically synthesized using a potassium hexafluorozirconate solution, reducing agents, and stabilizer or capping agents to control the growth of nanoparticles without aggregation (Bansal et al., 2011). Otherwise, biobased protocols for the synthesis of metal nanoparticles have been achieved using bacterial (Gowri et al., 2014), fungal (Bansal et al., 2004), yeast (Golnaraghi-Ghomi et al., 2021), or unicellular algae (Mandal et al., 2006) species. Thus, the metabolism of the microorganisms is relied upon for the biogenic production of the metal nanoparticles, intracellular or extracellular (Castro et al., 2014). In this type of biosynthesis, biomolecules isolated from microorganisms act as reducing or capping agents (Sintubin et al., 2012). This method of preparing metal nanoparticles offers lower costs and higher productivity (Parikh et al., 2008). The mechanistic pathways of the formation of nanoparticles, that is, ZrO2-NP with the aid of microorganisms, were proposed using the reactions of zirconium ions with biomolecules through hydrolysis of a zirconium salt solution (Tai et al., 2004) or molecular and dissociative mechanisms (Imanova et al., 2021). Many studies have focused on the significance of preparing and using nanoparticles from *F. oxysporum* extract because of its diverse and superior biological characteristics (Ahmad et al., 2002; Durán et al., 2005; Gholami-Shabani et al., 2014; Almeida et al., 2017; Vivekanandhan et al., 2018; Deepa & Panda, 2020).

In continuation of our recent work on the green synthesis of metal nanoparticles (Heikal et al., 2020) and medicinal applications (Zaghloul et al., 2017), we report a green biogenic protocol for the biosynthesis of zirconia dioxide nanoparticles from *F. oxysporum*. Consequently, the projected work was extended to characterize the stability performance of the biogenic ZrNPs and to evaluate their potency as cytotoxic agents against certain tumor and normal cell lines as well as their antimicrobial activities.

Materials and Methods

Fusarium oxysporum isolates were assembled from the Mycological Laboratory, Botany Department, Faculty of Science, Mansoura University, Mansoura, Egypt. GPS: 31.041898896810366, 31.353506232711727

PDA and MGYP media

Potato dextrose agar medium (PDA)(Griffith et al., 2007; Camelini et al., 2012) was prepared from potato extract (200g/L), dextrose (20g/L), and agar (20g/L). Maltose glucose yeast peptone medium (MGYP) (Apte et al., 1993; Koim-Puchowska et al., 2021) was prepared from malt extract (3g/L), glucose (10g/L), yeast extract (3g/L), and peptone (5g/L). All media were dissolved in 1L distilled water and autoclaved at 121°C for 20min, followed by cooling. The medium was mixed well before pouring.

Microorganism and culture conditions

F. oxysporum culture was carried out on a PDA medium, and the plates were subsequently incubated for 5 days at 25°C until there was sufficient fungal growth. The fungus culture was kept at 4°C to be used for further biosynthesis processes (Elamawi et al., 2018; Linh et al., 2021).

Synthesis of biobased species of F. oxysporum based on ZrNPs

The fungus was cultured as agar discs (three to five discs) in a liquid MGYP medium to obtain the purified biomass of *F. oxysporum.* Many discs of fresh culture were inoculated in Erlenmeyer flasks (500mL); each of these flasks contained an MGYP medium (100mL), which were then incubated with continuous shaking at 180rpm for 72h at 25±1°C. After the incubation period, the filtration step was performed to separate the fungal biomass from the medium. The fungal biomass was repeatedly washed with sterilized distilled water three times to remove any residual contamination from the medium. Next, 20g of wet mycelia were immersed in sterilized deionized water (100mL). The mixture was incubated under the same optimal conditions for 24h, and the pH was adjusted to 9 for the cell-free filtrate for each 100mL volume. Cautiously, a potassium hexafluorozirconate (K2ZrF6) solution was prepared at a concentration of 10^{-3} M. These flasks were stirred under the previously mentioned dark conditions to avoid photo-oxidation of zirconium ions. The control flasks (cell-free filtrate without

zirconium ions) were added under the same conditions. Many techniques have recently been reported for the biosynthesis of nanozirconium by the action of fungi species (Bansal et al., 2004; Li et al., 2011; Ghomi et al., 2019).

Potential cytotoxic activity

The cytotoxic activity of the biosynthesized ZrNP, K_2ZrF_6 solution, and doxorubicin as a standard anticancer drug were investigated in six tumor cell lines (HePG-2, HeLa, HEP2, PC3, MCF-7, and HCT-116) and a normal lung fibroblast cell line. Cell lines inspected were purchased from ATCC by a holding company for biological products and vaccines (VACSERA, Cairo, Egypt). RPMI-1640 medium, MTT, and DMSO were acquired from Sigma Co., St. Louis, USA, and fetal bovine serum (FBS) was purchased from GIBCO, UK.

Preparation of MTT solution

An MTT stock solution was prepared by dissolving 5mg of MTT in 1mL of phosphate-buffered saline (pH= 7.4). The solution was sterilized and aliquoted into 5mL tubes. The mixture was well-dissolved using a vortex or sonication. The prepared MTT solution is available to use for 6 months with storage at −20°C away from light.

Protocol of the MTT assay

Cell strains were grown in RPMI-1640 medium with 10% FBS. Penicillin (100 units/mL) and streptomycin (100µg/mL) were added at 37°C in a 5% CO_2 incubator. Cell lines were seeded in a 96-well plate at a density of 1.0×10^4 cells/well at 37°C for 48h under 5% CO_2. Cells were incubated and treated with various concentrations of the tested samples and successively incubated for an additional 24h. After 24h of drug treatment, 20µL of MTT solution (5mg/mL) was added, and the cells were incubated for 4h. A 100µL volume of DMSO was added to the individual wells to dissolve the generated violet formazan. The colorimetric assessment is reverential, and the absorbance of the color intensity was measured at λ= 570nm using a plate reader (EXL 800, USA). The absorbance reads were recorded, and the culture media background was subtracted from the absorbance reads for a corrected absorbance.

The % inhibitions were calculated as follows (Eq. 1) (Ertik et al., 2021):

$$\% \text{ Inhibition} = (100 \times (A \text{ control} - A \text{ sample})) \quad \text{(Eq. 1)}$$

IC_{50} values (µg/mL) were estimated from a nonlinear regression, sigmoid model, and analyzed using Origin 8.0® software (Origin Lab Corporation). The percentages of relative cell viability were calculated from the following equation (Eq.2):

$$\% \text{ Cell viability} = (A \text{ sample}/A \text{ control}) \times 100 \quad \text{(Eq. 2)}$$

Here, "A sample" signifies the absorbance of the sample, whereas "A control" signifies the absorbance of the control. The negative control was prepared by mixing the untreated cells with MTT solution and solubilizing buffer, whereas the blank sample was prepared by adding medium without cells with MTT solution and solubilizing buffer.

MIC

The minimum inhibitory concentration (MIC) test was conducted to investigate the antimicrobial potency of the biosynthesized ZrNPs prepared from the *F. oxysporum* extract by estimating microbial growth at a definite concentration of the tested sample. Thus, a macro dilution broth technique was used to conform to the requirements of the US Environmental Protection Agency. The sterilized nutrient broth medium prepared for the bacterial species and the Sabouraud broth prepared for the yeast were transferred to test tubes containing various concentrations of the ZrNP solution precisely inoculated with 0.1 mL of standard inoculum (10^7 CFU/mL). Next, the tubes containing the bacterial species were incubated for 24h at 37°C and those containing yeast for 24 to 48h at 30°C. Control tubes were prepared by adding growth medium, saline, and inoculum to each of the tested microbial species. The MIC was determined as the test tube sample that had no turbidity compared with the control sample. The MIC values (recorded in µg/mL) expressed the sample concentration responsible for the inhibition of the microbial species (Hassan et al., 2009). The investigated microbial species were obtained from the Microbiological Resources Center (Cairo Mircen, Egypt).

Instruments

The characteristic transmission electron microscopy (TEM) was conducted on a JEOL JEM-2100attached to a CCD camera at an acceleration voltage of 120kV (Tokyo, Japan) using a carbon-coated grid (Type G 200, 3.05µ

diameter, TAAP, USA), and the scanning electron microscopy (SEM) was conducted on a JEOL JSM, 6510 lv. The FT-IR spectrum was measured on a Thermo-Fisher Nicolet IS10spectrophotometer at the spectral analysis unit of Mansoura University, Mansoura, Egypt. UV-vis absorption spectroscopy was conducted using a Uni cam UV-VIS UV2. Energy-dispersive X-ray analysis (EDX) for elemental analysis was conducted using an X-ray microanalyzer (Oxford 6587, INCA) attached to a JEOL JSM-5500LV scanning electron microscope at 20kV.

Results and Discussion

Biosynthesis of nano-zirconia by F. oxysporum

To biosynthesize nano-zirconia, *F. oxysporum* (Fig. 1) was cultured on an MGYP broth medium for fungal biomass generation, the fungal biomass has a reddish-colored growth that was distinguished from the yellowish color of the control flask (MGYP medium only) (Fig. 2).

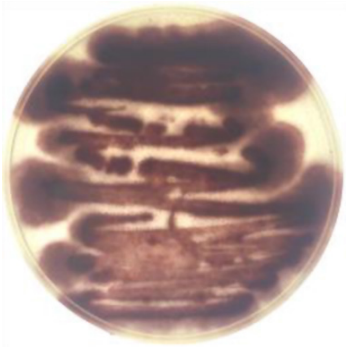

Fig. 1. The growth of *F. oxysporum* on PDA medium after incubation for 7 days at room temperature, the aerial hyphal growth appeared as a distinctive dark brown white color

Fig. 2. The growth of *F. oxysporum* on MGYP medium, mycelial mat generation in MGYP broth medium after incubation under incessant agitation conditions for 72h has a distinctive reddish color of this fungus [(A) is a control flask (MGYP medium without inoculum), (B) is a biomass-comprising flask]

Afterward, the incubation of the cell-free water extract and K_2ZrF_6 was accomplished and zirconia nanoparticles were synthesized. The visible conversion in color from pink to purple color was recognized as an indicator for the formation of nano-zirconia. This may happen due to a gradual reduction of zirconium ions to zero-state zirconium atoms (Fig. 3). The zirconia nanoparticles were separated by centrifuge the zirconia nanoparticles' solution at 13rpm for 10min (Fig. 4).

Fig. 3. The biogenic synthesized ZrNPs. The light violet color was changed to dark purple after 24h incubation [flask (A) is the control (cell-free filtrate without zirconia cations), and flask (B) is the test flask (cell-free filtrate with zirconia cations ZrF6)]

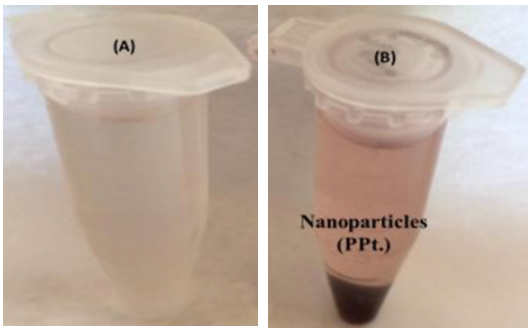

Fig. 4. Separation of zirconia nanoparticles [(A) is a control (cell-free filtrate without zirconium ions) and (B) is zirconia nanoparticles separated by centrifugation at 13rpm for 10min]

Characterization of the synthesized nanozirconia

UV-visible spectral analysis

Zirconium oxide nanoparticles have been widely biosynthesized and characterized using UV-visible spectra in recent years to study the optical properties and photocatalytic degradation of zirconia nanostructures (Kumari et al., 2009a; Kumari et al., 2009b; Zinatloo-Ajabshir & Salavati-Niasari, 2016; Al-Zaqri et al., 2021). ZrNPs produced by *F. oxysporum* were scanned using a UV-vis spectrum with a range scale of 200-400nm, in which a characteristic absorption peak at λ= 275nm was recorded. This peak is considered as an indication of the presence of biosynthesized nanozirconia (Fig. 5).

Transmission electron microscope

The TEM image of the biosynthesized ZrNPs was recorded at a magnification of 100nm. This analysis enables the determination of the surface morphology and the characteristic size distribution of ZrNPs (Siddiqui et al., 2012; Smith, 2015; Zinatloo-Ajabshir & Salavati-Niasari, 2016). The results specified that the size of the metal nanoparticles ranged from 5 to 15nm with spherical shapes. Most of the nanoparticles were aggregated, but others were non aggregated; this is related to the effect of the capping agent surrounding the nanoparticles arising from protein. Thus, the repulsion force between the nanoparticles is produced by the effect of the capping agent. The nanozirconia that appeared on the micrograph was a mainly spherical shape with the largest surface area (Fig. 6).

Selected area diffraction pattern analysis

The selected area diffraction pattern (SADP) technique is an experimental crystallographic analysis implemented along with TEM analysis (Mishra et al., 2020). In this technique, SADP was used to analyze a drop of the nanoparticle solution in the colloidal phase, in which the ZrNPs appeared as light spots in the diffraction pattern. Therefore, the nature of the nanoparticles is polycrystalline in form, and the diffraction rings indicated the formation of ZrNPs (Fig. 7).

SEM

The surface morphology of ZrNPs was determined via SEM analysis, a technique that images the surface through direct visualization with a scattering beam of electrons on the surface of the nanoparticles (Banu et al., 2018). This method offered several advantages for the surface morphology and size of the ZrNPs through the interaction of the electron beam with the atoms. The referred and recorded signals specified surface topography and sample composition information. The SEM micrograph in Fig. 8 shows nanoparticles aggregates. The SEM analysis showed that the surface structure of the ZrNPs ranged from 20 to 50nm in size, indicating the reducing capacity of the extract of *F. oxysporum*. The nanoparticles have mainly a spherical shape, devoid of any agglomeration without lineal interaction even with the aggregates, which signifies the stabilization of the nanoparticles by the capping agent.

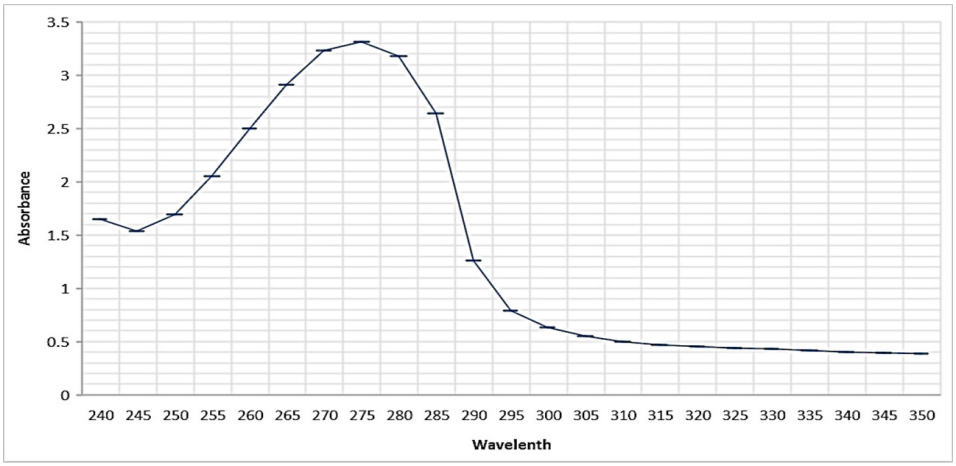

Fig. 5. UV-Vis spectral scan (from 200-400nm) of nano-zirconia biosynthesized by *F. oxysporum*

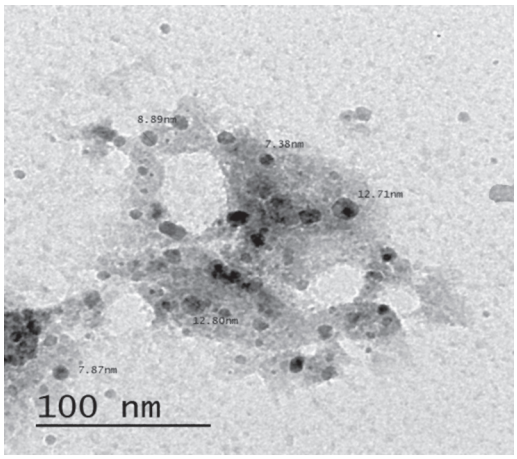

Fig. 6. TEM micrograph of biologically synthesized nano-zirconia by *F. oxysporum* [This image showed a spherical shape of nano-colloids and its size distribution range of (5-15)nm]

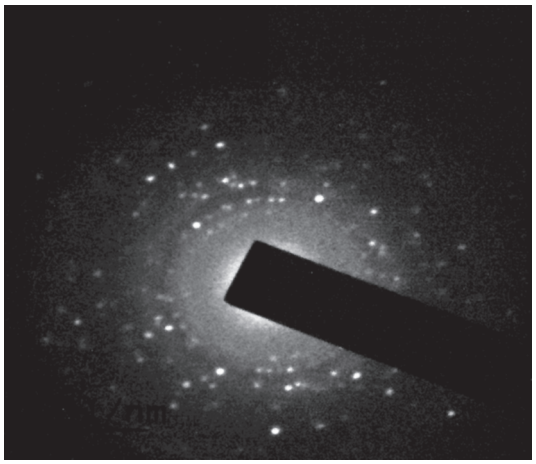

Fig. 7. Selected area diffraction pattern for zirconia nanoparticles, this micrograph showed the diffraction rings containing zirconia particles which appeared as lighted spots demonstrating the crystalline nature of zirconia nanoparticles

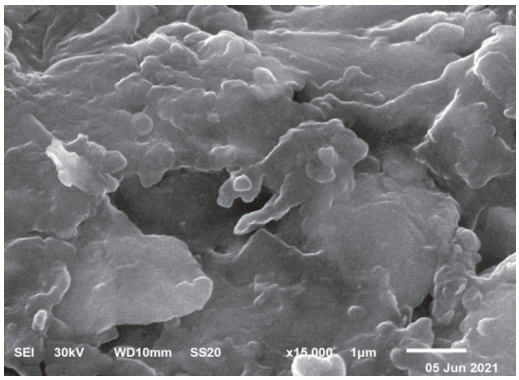

Fig. 8. Scanning electron microscopy image of zirconia nanoparticles

Energy dispersive analysis of X-ray (EDX)

EDX analysis is an x-ray performance applied to investigate the elemental composition of a definite material. The data recorded by this analysis showed a definite peak related to the element composition percentage referring to the correct composition of the analyzed sample. In this technique, the variance in electrons is filled by electrons transfer from a definite higher state, in which the x-ray is emitted through a balanced energy difference between the state of electrons. EDX analysis for ZrNPs (Mishra et al., 2020) as shown in Fig. 9 recorded in the spot-profile approach. The composition of the elements in the nano-solution that was determined by EDX spectra was expressed as weight percentages and found as followed: Si (0.50%), K (0.11%), Ca (2.33%), Zr (5.18%), C (53.39%), and O (38.50%). The optical absorption peak is detected at 2.2KeV, which specified the absorption of ZrNPs. Robust signals from the zirconium atoms are perceived, in line with weak signals for C, O, Si, K, and Ca elements are correspondingly verified. From the EDX spectrum, it is evident that ZrNPs produced

by *F. oxysporum* possess a percentage of zirconium weight. In addition, the results represented the composition of elements of the zirconia nanoparticles that were prepared by *F. oxysporum* as indicated by the EDX spectra.

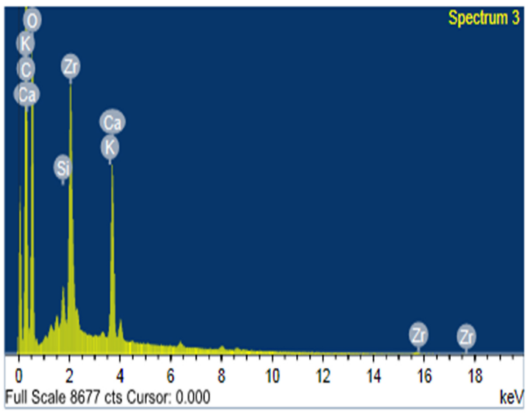

Fig. 9. EDX spectra of nano-zirconia [Zirconia X-ray radiation peaks are categorized specifying the reduction of zirconium cations and the formation of ZrNPs]

FT-IR spectroscopy

The FT-IR spectroscopic analysis was used to classify the functional groups of ZrNPs. The FT-IR spectroscopic analysis was used to study the changes in the functional groups of the *F. oxysporium* extract through reactions with zirconium cations to form zirconium dioxide, which indicated the formation of the ZrNPs in the solution. The spectrum signified a pattern of nanoparticles that involves absorption peaks that agree to the vibration frequencies between the bonds of the atoms in the ZrO_2 nanoparticles. The recorded values express the frequency of each defined group symbolled as "*v*," and the number of values is expressed in cm^{-1}. The scale of the FT-IR spectroscopic analysis is 400–4000cm^{-1} of the wave numbers through a relationship between the transmission % of the detected functional groups and the wave numbers identified for each group. Twenty-three absorption bands were recorded for the functional groups of the ZrNPs prepared using the extracted *F. oxysporium*, as shown in Table 1 and Fig. 10. The appearance of each absorption band was described as weak, medium, or strong, and broad or sharp bands. The values of the recorded transmission percentages are in high ranges. The recorded wave numbers are in the range of 422-3677cm^{-1}. The results of the FT-IR spectrum depend mainly on the types of the distinctive groups, the synthesis technique, and the solid-state structure of the analyzed sample. The results revealed distinctive absorption bands at *v*= 3677, 3649, and 3421cm^{-1} because of representative vibrations of the O–H stretching groups.

Additionally, the absorption bands due to N–H stretching, C–H stretching, and C–H bending groups appeared at *v*= 2926, 2857, and 1919cm^{-1}, respectively. The absorption bands at *v*= 1869, 1831, and 1742cm^{-1} are specifically assigned to the carbonyl groups, C=O stretching (conjugated acid halide), C=O anhydride, and C=O stretching (ester, six-membered lactone). The FT-IR analysis indicated the appearance of values for the aliphatic and aromatic alkene groups (C=C) at 1649 and 1520cm^{-1}, as well as vibration due to bending C–H groups; it was classified on the basis that it belongs to alkane groups at *v*= 1460 and 1420cm^{-1}, respectively. The results of the analysis also showed that there are definite absorption bands assigned for the stretching of CO (alkyl aryl ether) and the stretching of CO (primary alcohol) at *v*= 1239 and 1073cm^{-1}, allowing for the formation of metal–oxygen bonds. The generation of ZrO_2 was indicated by the presence of representative absorption bands in the region of *v*= 422–522cm^{-1} because of the vibration variations of the ZrO_3^{2-} groups (Vivekanandhan et al., 2010) and the absorption bands because of bending of the OH of phenols or carboxylic acids with peaks recorded at *v* = 131 and 1399cm^{-1}. The wave numbers at *v*= 793 and 815cm^{-1} are typical for the stretching vibration bands of the Zr–O bond. The IR spectrum indicated two bands at *v*= 1420 and 1460cm^{-1}, which are attributed to bending absorption bands of CH, which can be attributed to characteristic absorption bands because of the Zr–OC bonds. Briefly, the appearance of a new absorption band detected in the region *v*= 453cm^{-1} is an indication of the generation of a new absorption bond for metal ions with an oxygen atom (M–O vibration).

Potential biological evaluations

Cytotoxic activity of zirconia nanoparticles

The *in vitro* MTT colorimetric test was used to estimate the cytotoxic effects of the prepared zirconium dioxide nanoparticles. Recent research has focused on using the improved biological potency of zirconium dioxide and its nanoparticles for medical applications (Patil & Kandasubramanian, 2020). Furthermore, zirconium nanoparticles have been tested *in vivo* for cytotoxic assessment in fruit flies (Demir et al., 2013), *in vitro* for safety against placental cells (Lazić et al.,

2021), in cell-based assays (Sticker et al., 2015), for photoprotective potency (de Sá et al., 2021), and for assessment of genotoxic and apoptotic effects in L929 mouse fibroblast cell line (Atalay et al., 2018). The MTT procedure is a colorimetric assay that assesses the cytotoxic effects against living or viable cells, in which the reduction of the yellow color of the solution of 3-(4,5-dimethylthiazol-2-yl)-2,5-diphenyl tetrazolium bromide (MTT) to the blue insoluble formazan crystals is achieved by cellular enzymes. The number of viable cells is proportional to the reduction in MTT color to the respective blue formazan (Mosmann, 1983). In this case, the reduction step was affected by mitochondrial succinate dehydrogenases produced from living or viable cell lines. Six tumor cell lines were selected to evaluate the cytotoxic activity of the tested zirconium nanoparticles (HePG-2, MCF-7, HCT-116, PC3, HeP2, and HeLa cell lines), whereas the WI-38 cell line was selected as a normal cell line. Cytotoxicity results are summarized as inhibitive concentration IC_{50} values, which is the dose of the cytotoxic sample at which 50% viability was achieved. The results listed in Table 2 represent the cytotoxic results of zirconium nanoparticles with a standard solution of doxorubicin and potassium hexafluorozirconate (K_2ZrF_6) solution. Zirconium nanoparticles revealed moderate to weak cytotoxic effects in various tumor cell lines along with weak cytotoxicity in the WI-38 cell line. Specifically, zirconium nanoparticles demonstrated moderate cytotoxicity in HePG-2 (IC_{50}= 32.38µg/mL), MCF-7 (IC_{50}= 47.19µg/mL), PC3 (IC_{50}= 43.50µg/mL), HeP2 (IC_{50}= 38.23µg/mL), and HeLa (IC_{50}= 33.62µg/mL), complemented by weak cytotoxicity in HCT-116 (IC_{50}= 58.13µg/mL) and normal WI-38 cell lines (IC_{50}= 58.51µg/mL). The cytotoxicity results in various cell lines may be affected by the action of the remaining unreacted metal salt solution, so we have included the cytotoxic test using the potassium hexafluorozirconate (K_2ZrF_6) solution. Consequently, the results showed that the metal salt solution has moderate cytotoxic activity in HePG-2 (IC_{50}= 36.51µg/mL) only; however, its cytotoxic effects on the other tumor and normal cell lines have completely weak cytotoxic impacts: MCF-7 (IC_{50}= 56.41µg/mL), HCT-116 (IC_{50}= 66.61µg/mL), PC3 (IC_{50}= 54.63µg/mL), HeP2 (IC_{50}= 50.30µg/mL), HeLa tumor cell lines (IC_{50}= 52.87µg/mL), and the normal cell line WI-38 (IC_{50}= 70.30µg/mL).

TABLE 1. The data of FTIR spectrum of ZrNPs biosynthesized by the extracted *F. oxysporium*

Wave number (cm^{-1})	Characteristic groups	Appearance	Transmission %
422, 453	vibration of metal cations	medium	93.692
522	C-I stretching (halo compound)	strong	91.406
640	C-Br stretching (halo compound)	strong	92.250
1038	S=O stretching (sulfoxide)	strong	83.381
1073	C-O stretching (primary alcohol)	strong	82.445
1239	C-O stretching (alkyl aryl ether)	strong	89.326
1317	O-H bending (phenol)	medium	88.505
1339	S=O stretching (sulfate)	strong	88.040
1399	O-H bending (carboxylic acid)	medium	82.224
1420	C-H bending (alkane, methyl group)	medium	82.924
1460	C-H bending (alkane, methylene group)	medium	81.838
1520	C=C aromatic	weak	74.528
1543	N-O stretching (nitro compound)	strong	73.668
1649	C=C stretching (alkene, di-substituted (*cis*))	medium	68.483
1742	C=O stretching (ester, 6-membered lactone)	strong	83.506
1831	C=O anhydride	weak	95.934
1869	C=O stretching (conjugated acid halide)	strong	97.439
1919	C-H bending (aromatic compound)	weak	98.403
2857	C-H stretching	medium	83.115
2926	N-H stretching (amine)	strong, broad	78.840
3421	O-H stretching (alcohol)	strong, broad	65.944
3649	O-H stretching	strong, broad	84.245
3677	O-H stretching (alcohol)	medium, sharp	86.707

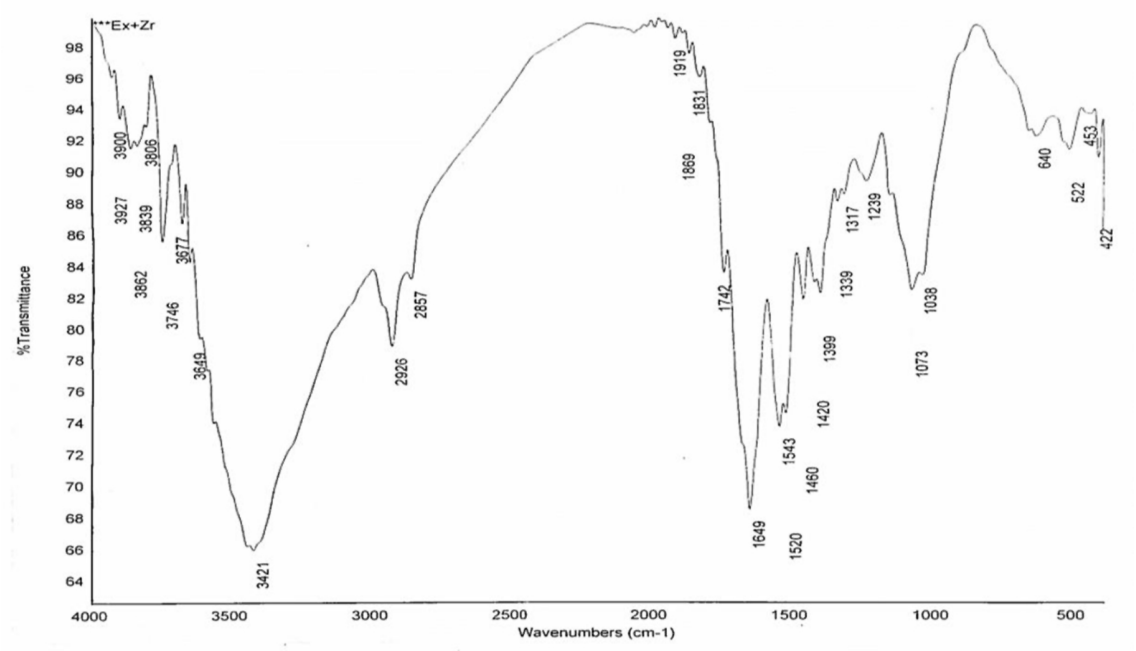

Fig. 10. The FT-IR spectrum of the synthesized zirconia nanoparticles prepared by the extracted *F. oxysporium*

TABLE 2. *In vitro* cytotoxicity of the biosynthesized ZrNPs

Samples	*In vitro* cytotoxicity, IC_{50} (µg/ mL) [a]						
	HePG-2	MCF-7	HCT-116	PC3	HeP2	HeLa	WI-38
Doxorubicin	4.5	4.17	5.23	8.87	8.54	5.57	16.09
ZrNPs	32.38	47.19	58.13	43.50	38.23	33.62	58.51
K_2ZrF_6 solution	36.51	56.41	66.61	54.63	50.30	52.87	70.30

[a] IC_{50} (µg/ mL): 1–10 (very strong), 11–20 (strong), 21–50 (moderate), 51–100 (weak) and > 100 (non-cytotoxic).

In contrast to the efficiency of the standard anticancer drug "doxorubicin" as a good inhibitor of cancer cell growth with very high efficiency, we found that this standard inhibitor has similar activity against the growth of normal cells, unlike nano-zirconium, which did not significantly affect the activity of normal cells and did not cause them severe damage. Hence, the importance of the new zirconium nanoparticles lies in the possibility of using it more in the future so that its efficiency as an inhibitor of the growth of cancer cells is improved by linking it to another substance chemically or improving the conditions that were applied when conducting the biological test to obtain another standard substance with high inhibition efficiency and high quality. The inhibition efficiency varies from one cell to another, and we found the order of the activity of the zirconium nanoparticles as follows: HePG-2 cell line is more applicable for the nature of the prepared zirconium nanoparticles with IC_{50}= 32.38 µg/ mL, this was accompanied by HeLa, HeP2, PC3, MCF-7, HCT-116, and WI-38 cell lines (Table 2).

All over again, the colorimetric MTT assay measures the cell metabolic activity depending on the reduction of tetrazolium dye MTT to its insoluble formazan caused by the effect of oxidoreductase enzymes contained viable cells. Predominantly, the inhibition percentage of ZrNPs, salt solution, and doxorubicin against human cancer, and normal cells was investigated at seven concentrations in the serial dilutions (1.56-100µg/ mL). The % inhibition measures the efficiency of the sample at a certain concentration to prevent cancer cells growth. In particular, the most potent % inhibition values were recorded at 100 µg/mL, in which the higher % inhibition (41.4%) was recorded for ZrNPs at this concentration on HePG-2, and Hela tumor cell lines. The % inhibition on the other tumor cells is found in the range 34.8-39.3%, while the % inhibition was recorded at a lower value on the normal WI-38 cell with 26.9%. Also, lower percentages were recorded than those

recorded for ZrNPs in the case of salt solution, which indicates the improvement of the inhibitory efficiency as a result of the formation of ZrNPs (Fig. 11).

Furthermore, the percentages of the average relative viability of cells at various concentrations (1.56 to 100µg/mL) of the prepared zirconium nanoparticles, the salt solution, and doxorubicin were studied against human cancer and normal cells. Cellular viability refers to the number of live healthy cells within a population that determines the overall health of cells, cellular survival, and metabolic changes associated with viable or nonviable cells. The cell viability assay can determine the loss of the cell membrane during cell death or physiological and biochemical activities suggestive of living cells. First, the viability percentage was calculated by adding the living and dead cells together to obtain a total cell count. Next, we divided the number of living cells by the total count of all cells to obtain the percentages of cellular viability. In contrast to measuring% inhibition, the determination of relative cell viability percentages, we found that the active and most active sample as an anticancer compound gave lower values of cell viability, just as we find that at high concentrations of the sample, there are lower percentages of live cells, which increases by decreasing the concentration of the sample (Fig. 12).

Antimicrobial activity

Table 3 shows the results of the MIC test for nanozirconia screened against bacterial species of *Klebsiella pneumoniae* (ATCC 10031), *Staphylococcus aureus* (ATCC 6538), *Escherichia coli* (ATCC 10536) bacterial species, and *Candida albicans* (EMCC number 105) fungal species. A serial dilution of the investigated nanozirconia solution was prepared at concentrations of 75, 50, and 25 µg/mL. The MIC results of metal nanoparticles prepared from the *F. oxysporum* fungus have recently been reported against various microbial species (Narayanan & Sakthivel, 2010; Ishida et al., 2014; Hashmi et al., 2019; Caruso et al., 2021). The MIC values indicated the minimum concentration required to allow for the highest growth of the microorganisms. Rather, it indicates the minimum concentration necessary to provide inhibitive growth of microorganisms. The control sample indicates the growth of the microbial strains without additives. In this method, we determined that the lowest percentage of turbidity indicated the highest percentage of inhibition for the growth of microorganisms.

The culture medium was prepared at a concentration of 20µL of microbial species per 2mL of the culture medium. The MIC results in Table 3 show that the sample possessed a MIC at 50 µg/mL in the tests against *K. pneumoniae*, *E.coli*, and *C. albicans*, whereas the MIC value was 25µg/mL against *S. aureus*. Therefore, concentrations of ZrNPs that inhibit the growth of the bacterial species were also able to inhibit the growth of the *C. albicans* species. The results are in agreement with our recently reported research on pathogenic, halophilic, and resistant bacterial species (Elsayed et al., 2016; Mohamedin et al., 2018; Elmogy et al., 2020; Ghoniem et al., 2021; Saber et al., 2021; Mowafy et al., 2021; Sultan et al., 2022).

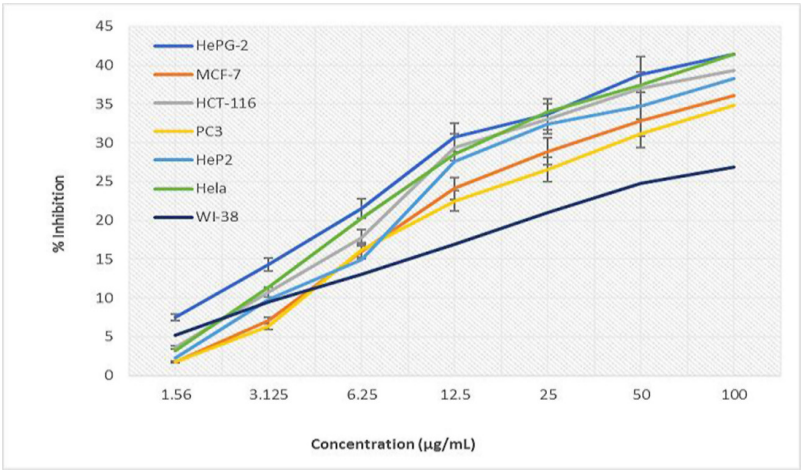

Fig. 11. % Inhibition plotted against the different concentrations of ZrNPs on the varied human tumor, and normal cell lines

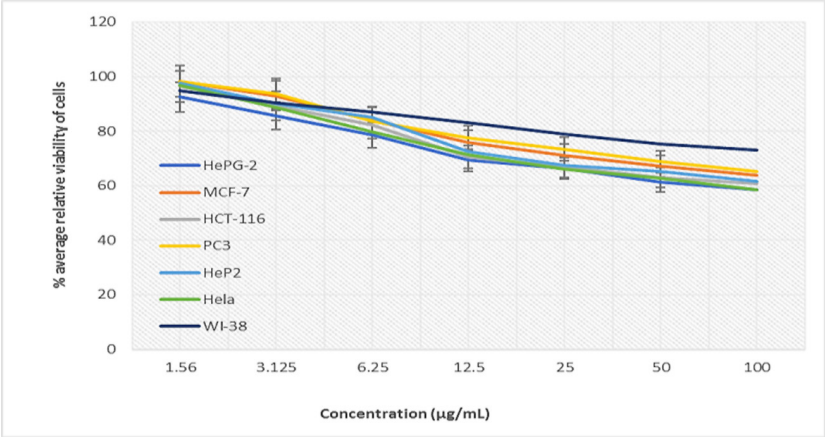

Fig. 12. % Average relative viability of cells plotted against the different concentrations of ZrNPs on the varied human tumor and normal cell lines

TABLE 3. MIC values of ZrNPs biosynthesized on the various microbial species

Microbial species	Concentration (µg/mL)			
	Control	75µg/mL	50µg/mL	25µg/mL
K. pneumoniae	2.33	1.608	**1.806**	2.33
S. aureus	2.38	1.0	1.848	**2.0**
E. coli	2.468	1.888	**1.988**	2.468
C. albicans	2.34	1.824	**2.0**	2.346

Conclusions

The biosynthesis of ZrNPs was achieved by reducing zirconium ions in the K_2ZrF_6 solution with *F. oxysporum* extract, in which the cytotoxicity and antimicrobial activities were evaluated. The results of cytotoxic activities in six tumor cell lines and a normal WI-38 cell line indicated moderate activities in HePG-2, MCF-7, PC3, HeP2, and HeLa cell lines with IC_{50} values ranging from 32.38 to 47.19µg/mL, along with weak cytotoxicity in the HCT-116 and WI-38 cell lines. The salt solution of $K2ZrF_6$ was also examined as a cytotoxic agent in the same cell lines with predominately weak cytotoxic effects and moderate cytotoxicity in the HePG-2 cell line, but still a weaker effect than the nanozirconia solution. Furthermore, ZrNPs revealed good antimicrobial activities with MIC values at 50 µg/mL against *K. pneumoniae*, *E. coli*, and *C. albicans*and 25µg/mL against *S. aureus*. The biological profile of nanozirconia solution lies in the fact that it has an inhibitory role in the growth of microbial and cancer cells with the possibility of avoiding serious damage to living cells in the case of anticancer potency, so it is possible to work on increasing their biological efficiency using some techniques in the future.

Conflict of interest: The authors state no conflict of interest.

Authors' contribution: Ashraf Elsayed and Attia A. Attia constructed the framework and helped in the practical work, data representation, writing, reviewing and editing. Ghada M. El-Shamy the master student who did the practical work and she participated in writing.

Ethical approval: Not applicable

References

Ahmad, A., Mukherjee, P., Mandal, D., Senapati, S., Khan, M.I., Kumar, R., Sastry, M. (2002) Enzyme Mediated Extracellular Synthesis of CdS Nanoparticles by the Fungus, *Fusarium oxysporum*. *Journal of the American Chemical Society,* **124**, 12108-12109.

Alagarsamy, A., Chandrasekaran, S., Manikandan, A. (2022) Green synthesis and characterization studies of biogenic zirconium oxide (ZrO_2) nanoparticles for adsorptive removal of methylene blue dye.

Journal of Molecular Structure, **1247**, 131275.

Almeida, É.S., de Oliveira, D., Hotza, D. (2017) Characterization of silver nanoparticles produced by biosynthesis mediated by *Fusarium oxysporum* under different processing conditions. *Bioprocess and Biosystems Engineering,* **40**, 1291–1303.

Almjasheva, O.V., Garabadzhiu, A.V.E., Litvinchuk, L.F., Dobritsa, V.P. (2017) Biological effect of zirconium dioxide-based nanoparticles. *Nanosystems: Physics, Chemistry, Mathematics*, **8**(3), 391-396.

Al-Zaqri, N., Muthuvel, A., Jothibas, M., Alsalme, A., Alharthi, F.A., Mohana, V. (2021) Biosynthesis of zirconium oxide nanoparticles using *Wrightia tinctoria* leaf extract: Characterization, photocatalytic degradation and antibacterial activities. *Inorganic Chemistry Communications,* **127**, 108507. https://doi.org/10.1016/j.inoche.2021.108507

Apte, P.S., Deshpande, M.V., Shankar, V. (1993) Optimization of medium for extracellular nuclease formation from *Rhizopus stolonifer*. *World Journal of Microbiology and Biotechnology*, **9**, 205-209.

Asadpour, E., Sadeghnia, H.R., Ghorbani, A., Sedaghat, M., Boroushaki, M.T. (2016) Oxidative stress-mediated cytotoxicity of zirconia nanoparticles on PC12 and N2a cells. *Journal of Nanoparticle Research*, **18**(1), 14.

Atalay, H., Çelik, A., Ayaz, F. (2018) Investigation of genotoxic and apoptotic effects of zirconium oxide nanoparticles (20nm) on L929 mouse fibroblast cell line. *Chemico-Biological Interactions,* **296**, 98-104. https://doi.org/10.1016/j.cbi.2018.09.017.

Bansal, V., Rautaray, D, Ahmada, A., Sastry, M. (2004) Biosynthesis of zirconia nanoparticles using the fungus *Fusarium oxysporum*. *Journal of Materials Chemistry,* **14**(22), 3303-3305.

Bansal, V., Ramanathan, R., Bhargava, S.K. (2011) Fungus-mediated biological approaches towards 'green' synthesis of oxide nanomaterials. *Australian Journal of Chemistry*, **64**(3), 279-293.

Banu, H., Renuka, N., Faheem, S., et al. (2018) Gold and silver nanoparticles biomimetically synthesized using date palm pollen extract-induce apoptosis and regulate p53 and Bcl-2 expression in human breast adenocarcinoma cells. *Biological Trace Element Research,* **186**(1), 122-134.

Bhardwaj, B., Singh, P., Kumar, A., Kumar, S., Budhwar, V. (2020) Eco-friendly greener synthesis of nanoparticles. *Advanced Pharmaceutical Bulletin*, **10**(4), 566.

Camelini, C.M., Pena, D.A., Gomes, A., Steindel, M., Rossi, M.J., Giachini, A.J., de Mendonça, M.M. (2012) An efficient technique for *in vitro* preservation of *Agaricus subrufescens* (=*A. brasiliensis*). *Annals of Microbiology*, **62**, 1279–1285.

Caruso, G.R., Tonani, L., Marcato, P.D., Kress, M.R.Z. (2021) Phenothiazinium photosensitizers associated with silver nanoparticles in enhancement of antimicrobial photodynamic therapy. *Antibiotics,* **10**, 569.

Castro, L., Blázquez, M.L., González, F.G., Ballester, A. (2014) Mechanism and applications of metal nanoparticles prepared by bio-mediated process. *Reviews in Advanced Sciences and Engineering*, **3**(3), 199-216.

Chau, T.P., Kandasamy, S., Chinnathambi, A., Alahmadi, T.A., Brindhadevi, K. (2021) Synthesis of zirconia nanoparticles using *Laurus nobilis* for use as an antimicrobial agent. *Applied Nanoscience*, 1-8. https://doi.org/10.1007/s13204-021-02041-w

da Silva, A.F.V., Fagundes, A.P., Macuvele, D.L.P, de Carvalho, E.F.U., Durazzo, M., Padoin, N., et al. (2019) Green synthesis of zirconia nanoparticles based on *Euclea natalensis* plant extract: Optimization of reaction conditions and evaluation of adsorptive properties. *Colloids and Surfaces A: Physicochemical and Engineering Aspects*, **583**, 123915.

de Sá, R.G., Arantes, T.M., de Macedo, E.F., Dona', L.M., Pereira, J.C.F., Hurtado, C.R., Varghese, R.J., Oluwafemi, O.S., Tada, D.B. (2021) Photoprotective activity of zirconia nanoparticles. *Colloids and Surfaces B: Biointerfaces,* **202**, 111636.

Deepa, K., Panda, T. (2020) Biogenic gold nanoparticles from *Fusarium oxysporum*: The impact of fungal morphology and localization studies. *Journal of Cluster Science,* **31**, 1185–1197.

Demir E, Turna F, Vales G, Kaya B, Creus A, and Marcos R. (2013). *In vivo* genotoxicity assessment of titanium, zirconium and aluminum nanoparticles, and their micro articulated forms, in Drosophila. *Chemosphere,* **93**(10), 2304-2310.

Durán, N., Marcato, P.D., Alves, O.L., *et al*. (2005) Mechanistic aspects of biosynthesis of silver nanoparticles by several *Fusarium oxysporum* strains. *Journal of Nanobiotechnology*, **3**, 8. https://doi.org/10.1186/1477-3155-3-8

Elamawi, R.M., Al-Harbi, R.E., Hendi, A.A. (2018) Biosynthesis and characterization of silver nanoparticles using *Trichoderma longibrachiatum* and their effect on phytopathogenic fungi. *Egyptian Journal of Biological Pest Control,* **28**, 28. https://doi.org/10.1186/s41938-018-0028-1

Elmogy, S., Ismail, M.A., Hassan, R.Y.A., Noureldeen, A., Darwish, H., Fayad, E., Elsaid, F., Elsayed, A. (2020) Biological insights of fluoroaryl-2,2'-bichalcophene compounds on multi-drug resistant *Staphylococcus aureus*. *Molecules*, **26**(1), 139. doi: 10.3390/molecules26010139.

Elsayed, A., Mohamedin, A., Ata, T., Ghazala, N. (2016) Molecular characterization of multidrug resistant clinical *Escherichia coli* isolates. *American Journal of Biochemistry and Molecular Biology,* **6**, 72-83.

Ertik, O., Kalındemirtaş, F.D., Kaya, B., Yanardag, R., Kuruca, S.E., Şahin, O., Ülküseven, B. (2021) Oxovanadium (IV) complexes with tetradentatethiosemicarbazones. Synthesis, characterization, anticancer enzyme inhibition and *in vitro* cytotoxicity on breast cancer cells. *Polyhedron*, **202**, 115192.

Gaafar, R., Diab, R., Halawa, M., Elshanshory, A., El-Shaer, A., Hamouda, M. (2020) Role of zinc oxide nanoparticles in ameliorating salt tolerance in soybean. *Egyptian Journal of Botany*, **60**(3), 733-747.

Gholami-Shabani, M., Akbarzadeh, A., Norouzian, D., et al. (2014) Antimicrobial activity and physical characterization of silver nanoparticles green synthesized using nitrate reductase from *Fusarium oxysporum*. *Applied Biochemistry and Biotechnology,* **172**, 4084–4098.

Ghomi, G., Reza, A., *et al*. (2019) Fungus-mediated extracellular biosynthesis and characterization of zirconium nanoparticles using standard *Penicillium* species and their preliminary bactericidal potential: A novel biological approach to nanoparticle synthesis. *Iranian Journal of Pharmaceutical Research (IJPR),* **18**(4), 2101-2110.

Ghoniem, A.A., Abd El-Hai, K.M., El-Khateeb, A.Y., Eldadamony, N.M., Mahmoud, S.F., Elsayed, A. (2021) Enhancing the potentiality of *Trichoderma harzianum* against *Pythium* pathogen of beans using Chamomile (*Matricaria chamomilla, L.*) flower extract. *Molecules*, **26**(4), 1178. doi: 10.3390/molecules26041178.

Golnaraghi-Ghomi, A.R., Mohammadi-Khanaposhti, M., Sokhansanj, A., Saadati, Y., Khazraei, E., Kobarfard, F., et al. (2021) Artificial neural network modeling of fungus-mediated extracellular biosynthesis of zirconium nanoparticles using standard *Penicillium* spp. *Journal of Cluster Science*, 1-15. https://doi.org/10.1007/s10876-021-02111-7.

Gowri, S., Gandhi, R.R., Sundrarajan, M. (2014) Structural, optical, antibacterial and antifungal properties of zirconia nanoparticles by biobased protocol. *Journal of Materials Science and Technology*, **30**(8), 782-790.

Griffith, G.W., Easton, G.L., Detheridge, A., Roderick, K., Edwards, A., Worgan, H.J., Nicholson, J., Perkins, W.T. (2007) Copper deficiency in potato dextrose agar causes reduced pigmentation in cultures of various fungi. *FEMS Microbiology Letters*, **276**(2), 165-71.

Hamouda, I.M. (2012) Current perspectives of nanoparticles in medical and dental biomaterials. *Journal of Biomedical Research*, **26**(3), 143-151.

Hashmi, S.S., Abbasi, B.H., Rahman, L., Zaka, M., Zahir, A. (2019) Phytosynthesis of organo-metallic silver nanoparticles and their anti-phytopathogenic potency against soil borne *Fusarium* spp. *Materials Research Express,* **6**(11), 1150-9.

Hassan, A., Rahman, S., Deeba, F., Mahmud, S. (2009) Antimicrobial activity of some plant extracts having hepatoprotective effects. *Journal of. Medicinal Plants Research*(JMPR), **3**(1), 20-23.

Hayat, S.M.G., Bianconi, V., Pirro, M., Sahebkar, A. (2019) Stealth functionalization of biomaterials and nanoparticles by CD47 mimicry. *International Journal of Pharmaceutics*, **569**, 118628.

Heikal, Y.M., Sutan, N.A., Rizwan, M., Elsayed, A. (2020) Green synthesized silver nanoparticles induced cytogenotoxic and genotoxic changes in *Allium cepa* L. varies with nanoparticles doses and duration of exposure. *Chemosphere*, **243**, 125430. doi: 10.1016/j.chemosphere.2019.125430.

Imanova, G.T., Agayev, T.N., Jabarov, S.H. (2021) Investigation of structural and optical properties of zirconia dioxide nanoparticles by radiation and thermal methods. *Modern Physics Letters B*, **35**(02), 2150050.

Ingale, A.G., Chaudhari, A.N. (2013) Biogenic synthesis of nanoparticles and potential applications: an eco-friendly approach. *Journal of Nanomedicine & Nanotechnology*, **4**(165), 1-7.

Iravani, S., Korbekandi, H., Mirmohammadi, S.V., Zolfaghari, B. (2014) Synthesis of silver nanoparticles: Chemical, physical and biological methods. *Research in Pharmaceutical Sciences*, **9**(6), 385.

Ishida, K., Cipriano, T.F., Rocha, G.M., Weissmüller, G., Gomes, F., Miranda, K., Rozental, S. (2014) Silver nanoparticle production by the fungus *Fusarium oxysporum*: Nanoparticle characterization and analysis of antifungal activity against pathogenic yeasts. *Memórias do Instituto Oswaldo Cruz,* **109**(2), 220-228.

Jamkhande, P.G., Ghule, N.W., Bamer, A.H., Kalaskar, M.G. (2019) Metal nanoparticles synthesis: An overview on methods of preparation, advantages and disadvantages, and applications. *Journal of Drug Delivery Science and Technology*, **53**, 101174.

Koim-Puchowska, B., Kłosowski, G., Drozdz-Afelt, J.M., Mikulski, D., Zielinska, A. (2021) Influence of the medium composition and the culture conditions on surfactin biosynthesis by a native *Bacillus subtilis*natto BS19 Strain. *Molecules* **26**, 2985. https://doi.org/10.3390/molecules26102985

Kumari, L., Du, G.H., Li, W.Z., Vennila, R.S., Saxena, S.K., Wang, D.Z. (2009a) Synthesis, microstructure and optical characterization of zirconium oxide nanostructures. *Ceramics International,* **35**(6), 2401-2408.

Kumari, L., Li, W., Xu, J., Leblanc, R., Wang, D., Li, Y., Guo, H., Zhang, J. (2009b) Controlled hydrothermal synthesis of zirconium oxide nanostructures and their optical properties. *Crystal Growth & Design,* **9**(9), 3874-3880.

Lazić, V., Pirković, A., Sredojević, D., Marković, J., Papan, J., Ahrenkiel, S.P., Janković-Častvan, I., Dekanski, D., Jovanović-Krivokuća, M., Nedeljković, J.M. (2021) Surface-modified ZrO_2 nanoparticles with caffeic acid: Characterization and *in vitro* evaluation of biosafety for placental cells. *Chemico-Biological Interactions,* **347**, 109618.

Li, X., Xu, H., Chen, Z-S., Chen, G. (2011) Biosynthesis of nanoparticles by microorganisms and their applications. *Nanostructures for Medicine and Pharmaceuticals,* **2011**, Article ID 270974. https://doi.org/10.1155/2011/270974

Linh, T.M., Mai, N.C., Hoe, P.T., Ngoc, N.T., Thao, P.T.H., Ban, N.K., Van, N.T. (2021) Development of a cell suspension culture system for promoting alkaloid and vinca alkaloid biosynthesis using endophytic fungi isolated from Local *Catharanthus roseus*. *Plants,* **10**, 672. https://doi.org/10.3390/plants10040672

Mandal, D., Bolander, M.E., Mukhopadhyay, D., Sarkar, G., Mukherjee, P. (2006) The use of microorganisms for the formation of metal nanoparticles and their application. *Applied Microbiology and Biotechnology*, **69**(5), 485-492.

Mishra, A.K., Tiwari, K.N., Nath, G. (2020) Green synthesis of silver nanoparticles from leaf extract of *Nyctanthes arbortristis* L. and assessment of its antioxidant, antimicrobial response. *Journal of Inorganic and Organometallic Polymers and Materials,* **30**, 2266-2278.

Mohamedin, A.H., Mowafy, A.M., Elsayed, A., Ghanim, S.O. (2018) Potential applications of some moderate halophilic bacteria. *Egyptian Journal of Aquatic Biology and Fisheries*, **22**(5), 537–550.

Mosmann, T. (1983) Rapid colorimetric assay for cellular growth and survival: application to proliferation and cytotoxicity assays. *Journal of Immunological Methods,* **65**(1-2), 55-63.

Mowafy, A.M., Fawzy, M.M., Gebreil, A., Elsayed, A. (2021) *Endophytic Bacillus*, *Enterobacter*, and *Klebsiella* enhance the growth and yield of maize. *Acta Agriculturæ Scandinavica Section B Soil and Plant Science*, **71**(4), 237–246.

Narayanan, K.B., Sakthivel, N. (2010) Biological synthesis of metal nanoparticles by microbes. *Advances in Colloid and Interface Science*, **156**(1-2), 1-13.

Osborne, E.A., Atkins, T.M., Gilbert, D.A., Kauzlarich, S.M., Liu, K., Louie, A.Y. (2012) Rapid microwave-assisted synthesis of dextran-coated iron oxide nanoparticles for magnetic resonance imaging. *Nanotechnology*, **23**(21), 215602.

Panigrahi, S., Kundu, S., Ghosh, S., Nath, S., Pal, T. (2004) General method of synthesis for metal nanoparticles. *Journal of Nanoparticle Research*, **6**(4), 411-414.

Parikh, R.Y., Singh, S., Prasad, B.L.V., et al (2008) Extracellular synthesis of crystalline silver nanoparticles and molecular evidence of silver resistance from *Morganella sp*.: Towards understanding biochemical synthesis mechanism. *Chem Bio Chem,* **9**, 1415–1422.

Patil, M.P., Kim, G.D. (2018) Marine microorganisms for synthesis of metallic nanoparticles and their biomedical applications. *Colloids and Surfaces B: Biointerfaces*, **172**, 487-495.

Patil, N.A., Kandasubramanian, B. (2020) Biological and mechanical enhancement of zirconium dioxide for medical applications. *Ceramics International,* **46**(4), 4041-4057.

Saber, W.E.I.A., El-Naggar, N.E-A., El-Hersh, M.S., El-Khateeb, A.Y., Elsayed, A., Eldadamony, N.M., Ghoniem, A.A. (2021) Rotatable central composite design versus artificial neural network for modeling biosorption of Cr^{6+} by the immobilized *Pseudomonas alcaliphila* NEWG-2. *Scientific Reports*, **11**(1), 1717. https://doi.org/10.1038/s41598-021-81348-8

Sarma, H., Joshi, S.J., Prasad, R., Jampilek, J. (2021) Biobased nanotechnology for green applications. 1st ed., Nanotechnology in the Life Sciences Series, Springer.

Siddiqui, M.R.H., Al-Wassil, A.I., Al-Otaibi, A.M., Mahfouz, R.M. (2012) Effects of precursor on the morphology and size of ZrO_2 nanoparticles, synthesized by sol-gel method in non-aqueous medium. *Materials Research,* **15**(6), 986-989.

Singh, P., Kim, Y.J., Wang, C., Mathiyalagan, R., Yang, D.C. (2016) *Weissella oryzae* DC6-facilitated green synthesis of silver nanoparticles and their antimicrobial potential. *Artificial Cells, Nanomedicine and Biotechnology,* **44**(6), 1569-1575.

Sintubin, L., Verstraete, W., Boon, N. (2012) Biologically produced nanosilver: current state and future perspectives. *Biotechnology & Bioengineering,* **109**, 2422–2436.

Smith, DJ. (2015) Chapter 1: Characterization of nanomaterials using transmission electron microscopy. In: "*Nanocharacterization*", (2), pp. 1-29. doi: 10.1039/9781782621867-00001

Sticker, D., Rothbauer, M., Charwat, V., Steinkühler, J., Bethge, O., Bertagnolli, E., Wanzenboeck, H.D., Ertl, P. (2015) Zirconium dioxide nanolayer passivated impedimetric sensors for cell-based assays. *Sensors and Actuators B: Chemical*, **213**, 35-44.

Sultan, M.S., Elsayed, A., El-Amir, Y.A. (2022) *In vitro* effect of plant parts extract of *Senecio glaucus* L. On pathogenic bacteria. *Biointerface Research in Applied Chemistry*, **12**(3), 3800–3810.

Tai, C.Y., Hsiao, B.Y., Chiu, H.Y. (2004) Preparation of spherical hydrous-zirconia nanoparticles by low temperature hydrolysis in a reverse microemulsion. *Colloids and Surfaces A: Physicochemical and Engineering Aspects*, **237**(1-3), 105-111.

Valencia, P.M., Farokhzad, O.C., Karnik, R., Langer, R. (2012) Microfluidic technologies for accelerating the clinical translation of nanoparticles. *Nature Nanotechnology*, **7**(10), 623-629.

Vivekanandhan, P., Deepa, S., Kweka, E.J., et al. (2018) Toxicity of *Fusarium oxysporum*-VKFO-01 derived silver nanoparticles as potential inseciticide against three mosquito vector species (Diptera: Culicidae). *Journal of Cluster Science*, **29**, 1139–1149.

Vivekanandhan, S., Venkateswarlu, M., Rawls, H.R., Satyanarayana, N. (2010) Acrylamide assisted polymeric citrate route for the synthesis of nanocrystalline ZrO_2 powder. *Materials Chemistry and Physics,* **120**, 148-154.

Yadav, L.R., Ramakrishnappa, T., Pereira, J.R., Venkatesh, R., Nagaraju, G. (2022) Rubber latex fuel extracted green biogenic nickel doped ZrO_2 nanoparticles and its resistivity. *Materials Today: Proceedings*, **49**, 681-685..

Zaghloul, H., El Morsi, A.A., Soweha, H.E., Elsayed, A., Seif, S., El-Sharawy, H. (2017) A simple real-time polymerase chain reaction assay using SYBR Green for hepatitis C virus genotyping. *Archives of Virology,* **162**(1), 57-61.

Zinatloo-Ajabshir, S., Salavati-Niasari, M. (2016) Zirconia nanostructures: Novel facile surfactant-free preparation and characterization. *International Journal of Applied Ceramic Technology*, **13**(1), 108-115. https://doi.org/10.1111/ijac.12393.

التخليق الحيوي وتوصيف وتقييم جزيئات الزركونيا النانوية بواسطة أنواع من فيوزاريوم أوكسيسبوروم كعوامل جديدة محتملة مضادة للميكروبات والسموم الخلوية

أشرف السيد[1]، غادة محمد الشامي[2]، عطيه احمد عطيه[2]

[1]قسم النبات- كلية العلوم- جامعة المنصورة- المنصورة- مصر، [2] قسم النبات والميكروبيولوجي- كليه العلوم- جامعه بنها- بنها- مصر.

في هذا البحث، تم التخليق الحيوي لجسيمات الزركونيا النانوية باستخدام محلول سداسي فلوروزركونات البوتاسيوم مع مستخلص فطر فيوزاريوم أوكسيسبوروم. كما تم التحقق من تكوين جزيئات النانو زركونيا عن طرق العديد من التحاليل الطيفية، ومن خلال دراسة حجم الجزيئات وطبيعتها وأشكال تجمعها. على الجانب الآخر، تم تقييم محلول النانو زركونيا كمضاد لنمو الخلايا السرطانية معمليا عن طريق تطبيقه بتركيزات عديدة على سته انواع من الخلايا السرطانية HePG-2 وMCF-7 وPC3 وHeP2 وHeLa ونوع من الخلايا الغير مصابة WI-38 باستخدام طريقة MTT اللونية. أشارت النتائج إلى أنشطة معتدلة على مختلف الخلايا السرطانية بقيم IC_{50} تتراوح من 32.38 إلى 47.19 ميكروغرام/ مل، جنبًا إلى جنب مع السمية الخلوية الضعيفة على خطوط الخلايا HCT-116 و WI-38عند IC_{50}= 58.13 و 58.51 على التوالي. علاوة على ذلك، أظهرت نتائج الاختبارات عند تقييم محلول النانو زركونيا كمضاد للميكروبات نشاطًا جيدًا مع MIC عند 50 ميكروغرام/ مل ضد *K. pneumoniae* و *E. coli* و *C. albicans*، بينما تم توثيق MIC عند 25 ميكروغرام/ مل ضد *S. aureus*. ومن ثم، تعكس الخواص البيولوجية لمحلول النانو زركونيا دورًا مثبطًا في نمو الخلايا الميكروبية والسرطانية مع إمكانية تجنب حدوث أضرار جسيمة للخلايا الحية في حالة الفاعلية المضادة للسرطان، وبالتالي فمن الممكن العمل على زيادة كفاءته البيولوجية باستخدام بعض التقنيات في المستقبل.